Open access • Journal Article • DOI:10.1086/154788

Pulsar average wave forms and hollow-cone beam models — Source link

D. C. Backer

Institutions: Goddard Space Flight Center

Published on: 01 Nov 1976 - The Astrophysical Journal

Topics: Pulsar and Beam (structure)

X-693-75-138
PREPRINT

NASA TM X- 70917

PULSAR AVERAGE WAVEFORMS AND HOLLOW-CONE BEAM MODELS

D. C. BACKER

JUNE 1975

GSFC

GODDARD SPACE FLIGHT CENTER
GREENBELT, MARYLAND

PULSAR AVERAGE WAVEFORMS AND HOLLOW-CONE BEAM MODELS

D.C. Backer*
Goddard Space Flight Center
Greenbelt, Maryland 20770

Received_____

*NAS/NRC Resident Research Associate

Address correspondence to

D.C. Backer
Radio Astronomy Branch, Code 693
Goddard Space Flight Center
Greenbelt, Maryland 20770

ABSTRACT

Analysis of pulsar average waveforms at radio frequencies from 40 MHz to 15 GHz based on the hypothesis that the observer sees one cut of a hollow-cone beam pattern and that stationary properties of the emission vary over the cone is presented. We find that the distributions of apparent cone widths, appropriately defined, for different observed forms of the average pulse profiles (SINGLE, DOUBLE/UNRESOLVED, DOUBLE/RESOLVED, TRIPLE and MULTIPLE), are in modest agreement with a model of a circular hollow-cone beam with random observer-spin axis orientation and random cone axis-spin axis alignment, and a small range of physical hollow-cone parameters for all objects. The agreement is not affected by considering the elliptical hollow-cone beam suggested in the work of Sturrock (1971) and Ruderman and Sutherland (1975).

Subject headings: pulsars

I. Introduction

The radiation from most pulsars arrives within a region of 5 per cent of the primary pulse period. Two outstanding features of the radiation are perfect symmetry of all aspects of observations, taken as an ensemble, under a time reversal and the division of the emission region into two regions in roughly half of the objects studied in detail. The time-reversal symmetry in the pulsar sample is an obvious result of emission models with a rotating beam (Gold 1968); we return to a discussion of models below following a discussion of our knowledge of the bifurcation of emission regions.

PSR 1919+21, the original pulsar (Hewish et al. (1968)) has an average waveform, or pulse profile, consisting of two peaks which identifies the presence of two components of the waveform (Drake 1968). The two-component, total-intensity average profile is now recognized in many pulsars: Smith (1972) categorizes 7 of 39 pulsars as "double pulse shape", while 4 of the objects display multiple (> 2) - component profiles. In previous work (Backer 1970a, 1970b, 1973 (Paper I); Backer, Rankin and Campbell 1975 (Paper II)) we show that total-intensity fluctuation profiles, measures of the variation of the second moment of the data about the mean, also display a bifurcation, even in cases where the average waveform only suggests

the presence of two components (e.g., see discussion of PSR2016+28 in Paper I). Also in the work just referenced several objects are studied for which, while displaying evidence of three components in the average and fluctuation profiles, the outer pair of components display more nearly common fluctuation properties when compared to the central component, as if a third pulse component were added to a more common double profile (e.g., PSR1237+25 and PSR1929+10 in Paper I and PSR1604-00 in Paper II). We are led naturally to consider these objects a subset of the basic double category due to the similarity of the outer pair of components. For the present purposes we ignore details such as "notches" in PSR1919+21 (Cordes 1975) and the bifurcation of each of the outer two components in PSR1327+25 (Paper I). Very few objects display more than the three prominent components in the principal emission region as outlined above.

There are two slight, but significant variations of average waveforms with radio frequency: first, the intensity ratios of components may vary with frequency indicating different flux-density spectra for components of a profile (e.g., Rankin et al. 1971, Manchester 1971c, Backer 1972); second, the separations of the peaks of components and the widths of single profiles, or components, often decrease with increasing frequency (Craft and Comella 1968), although some authors have reported the reverse effect (Craft 1970, Lyne, Smith and Graham 1971).

We return now to the other outstanding feature of pulsar radiation: the time-reversal symmetry and its interpretation in rotating-beam models. The rotating-beam models are further supported by the characteristic swing of the linear polarization vector across the pulse emission region first recognized by Radhakrishnan and Cooke (1969). In the latter work the authors establish the hypothesis that the radiation beam is a cone collinear with a dipole magnetic field axis and at some angle with respect to the rotation axis. Komesaroff (1970) develops the Radhakrishnan model and proposes a hollow-cone beam which explains the double nature of some average waveforms. Observers see a single or double average waveform depending on the difference of the observer and cone-axis polar angles and the hollow-cone beam parameters. If we fix the beam parameters for ensemble of pulsars, then the distribution of observed pulse widths is simply related to the distribution of cone-axis inclinations. Henry and Paik (1969) determine this distribution for a random orientation of cone axes.

Similar hollow-cone models are developed by Sturrock (1971) who predicts a spin-frequency dependence of the overall cone widths (Roberts and Sturrock 1972, 1973), and by Tademaru (1971) who considers the radio-frequency dependence of the cone widths. A related, but crude model for the spin-frequency dependence of cone-widths was first given by Gunn and Ostriker (1970). Eastlund (1968) also proposed a hollow-cone

emission beam and considered its radio-frequency dependence in another context. The recent work of Ruderman and Sutherland (1975) on hollow-cone emission beams aligned with an oblique magnetic dipole axis provides fresh impetus to exploring the consistency between the observations and the general concepts inherent to these models.

II. ANALYSIS

We are led by the observations and beam models outlined above to hypothesize the following criteria for inspecting pulsar radiation:

(1) The averaged beam pattern is a hollow-cone, perhaps with a pencil beam in the center, which revolves around the rotation axis. The observer is randomly oriented with respect to the rotation axis at an angle θ_o and the cone axis is either randomly oriented or randomly aligned with respect to the rotation axis at an angle θ_m. The average waveforms, or profiles, for several observer orientations are given in figure 1 which gives a schematic of the proposed beam geometry.

(2) The radio spectrum of the radiation can vary over the cone leading to a variation of the intensity ratios of profile components with frequency, when individual components are detectable.

(3) The observed, or apparent, cone width at maximum intensity (ϕ_o) and the cone thickness at half maximum (ϕ_c), as well as the pencil beam width at half maximum (ϕ_p), vary from object to object and are weakly related to the inverse of the radio frequency. The variation of apparent cone widths may arise from a range of physical cone widths or from the random angles (θ_o, θ_m) discussed in (1).

(4) The fluctuation statistics and the polarized Stokes parameters can vary across the cone. This information can corroborate the presence of components in the DOUBLE/UNRESOLVED category (fig. 1) and in objects with large ϕ_c and ϕ_p, or small ϕ_o. In the DOUBLE/RESOLVED and TRIPLE categories there is often rough mirror symmetry of these two properties of the radiation about the midpulse point.

(5) We allow for a category of more complex profiles with MULTIPLE components which do not fit at present the simple forms in figure 1.

An extensive list of pulsar observations, both published and unpublished (table 1), has been investigated following the above criteria. Since items (2) and (3) above mention significant dependences on radio frequency, the wide frequency range covered by these observations is essential to the investigation. The discussion below is confined to objects for which total intensity or circular-polarization data were available over an octave of radio frequency and usually from more than one independent observer. Due to the limited frequency coverage and sensitivity for some pulsars, it is possible that the statements concerning a few objects below may be altered upon further study.

The first step performed was measurement of <u>apparent half-power beamwidths</u>, ϕ, of the profiles of each object over the available range

of frequency. This width, in degrees[1], is $(\phi_o + \phi_c)$ in figure 1, or, more generally:

(1) the full width at half-maximum for SINGLE(S) profiles;

(2) the separation of half-maximum points on the leading and trailing edges for the estimated components in the first and second halves of DOUBLE/UNRESOLVED (DU) profiles, respectively;

(3) the same definition as in (2) for the first and last components of DOUBLE/RESOLVED (DR), TRIPLE (T) and MULTIPLE(M) profiles.

The measurements for a given object followed different of the above prescriptions at different radio frequencies due to the frequency dependence of profiles.

In figures 2a-d we present apparent half-power beamwidths for objects with measurements extending over at least two octaves of radio frequency. A schematic profile is given at the top of each plot with an indication of the quantity measured. For the DU, DR and T cases we identify two (I,II), or three (I,II,III),components and indicate by the same symbols when one, or two, of the components dominate the measurement, respectively. All measurements are accurate to ten percent, or less, except when flagged with error bars. These

[1]360 degrees = one pulse period.

observations are discussed individually in the Appendix.

On the basis of this multifrequency profile investigation, as well as fluctuation and polarization analyses discussed in other work, we group the objects into three categories:

S - SINGLE

DU - DOUBLE/UNRESOLVED

C - DOUBLE/RESOLVED, TRIPLE, and MULTIPLE.

The form of total intensity pulse profiles presented above is displayed in figure 3. All profiles are displayed on identical longitude scales. The profiles in the left three columns display an increasing width from 5-10° to nearly 40° as one progresses down each column with similar form within each column. Taking this one step further in width for the third category, we give in figure 4 the average profiles of two objects with exceptionally wide pulses (see also Backer, Boriakoff and Manchester 1973 and Davies et al. 1973.) In the case of PSR1541+09, we again find a predominantly double profile, at 1440 MHz, which is ten times wider than that of PSR0834+06 (fig. 3). Such a scaling of pulse-profile width with constant form is an obvious feature of oblique, hollow-cone emission patterns if we allow for random orientation of the cone axis.

Each object categorized was given a pulse width at the radio frequency most representative of its form, generally between 400 and

1400 MHz. These are summarized in the three histograms of figure 5. This summary indicates that the narrowest pulse beam widths are SINGLE, that the C widths are, on average, more than twice as wide as the S widths, and that the DU profiles are wider than the most common C widths.

III. COMPARISON TO MODEL

We compare now the observed distribution of pulse widths and forms with the hollow-cone model assuming:

(1) all pulsars have identical hollow-cone beams centered on the cone axis with openings Φ_o and thicknesses Φ_c, where (Φ_o, Φ_c) are the values of (ϕ_o, ϕ_c) that an observer would measure for cone and observer axes perpendicular to the spin axis (see fig. 1);

(2) the observer is randomly oriented in space with a polar angle θ_o measured from the rotation axis. The probability density for θ_o is thus $p_1(\theta_o) = (\sin \theta_o)/2$ for $0 \leq \theta \leq \pi$;

(3) the cone axis is either randomly oriented or randomly aligned with respect to the rotation axis at a polar angle θ_m. The latter case has not been treated in the past (Henry and Paik 1969, Roberts and Sturrock 1972, 1973), but could be relevant physically if alignment and disalignment torques have operated on the angle θ_m. The probability densities for these two cases are $p_2(\theta_m) = (\sin \theta_m)/2$ and $p_2'(\theta_m) = 1/\pi$, respectively, for $0 \leq \theta_m \leq \pi$.

Since the angles θ_o and θ_m are surely independent, the probability density for θ_o and θ_m $p(\theta_o, \theta_m)$ is simply the product $p_1(\theta_o)\ p_2(\theta_m)$. It

is useful to determine the probability density $p(\theta_m, \delta \equiv \theta_o - \theta_m)$ which is simply $p_1(\theta_m + \delta)\ p_2(\theta_m)$. From $p(\theta_m, \delta)$ one can find $p(\phi, \delta)$ using the transformation $\frac{\partial(\theta_m, \delta)}{\partial(\phi, \delta)}$ and the spherical triangle relation between θ_m, δ and ϕ:

(1) $$\cos(\Phi/2) = \cos\theta_m \cos(\theta_m - \delta) + \sin\theta_m \sin(\theta_m - \delta)\cos(\phi/2)$$

where $\Phi \equiv \Phi_o + \Phi_c$.

It is our hypothesis that the histograms in figure 5 are the consequences of observations where $|\delta|$ is roughly constant. For the C histogram we propose $\delta \approx 0$ and therefore compare the data to $p(\phi, 0)$:

(2)
$$p(\phi,0)\, d\phi = \frac{1}{8} \frac{(1-\cos(\Phi/2))^{3/2}}{(1-\cos(\phi/2))^{2}} \frac{\sin(\phi/2)}{(\cos(\Phi/2) - \cos(\phi/2))^{1/2}} \begin{pmatrix}\text{random}\\ \text{orientation}\end{pmatrix}$$

$$\frac{1}{4\pi} \frac{(1-\cos(\Phi/2))}{(1-\cos(\phi/2))^{3/2}} \frac{\sin(\phi/2)}{(\cos(\Phi/2) - \cos(\phi/2))^{1/2}} \begin{pmatrix}\text{random}\\ \text{alignment}\end{pmatrix}$$

which are valid for $\Phi \le \phi \le 2\pi$.

The cumulative probabilities $P(\phi)$ are:

(3)
$$P(\phi) = \frac{1}{4}\left[\frac{(\cos(\Phi/2) - \cos(\phi/2))^{1/2}(1-\cos(\Phi/2))^{1/2}}{(1-\cos(\phi/2)} + \tan^{-1}\left(\frac{\cos(\Phi/2) - \cos(\phi/2)}{1 - \cos(\Phi/2)}\right)^{1/2}\right], \text{ and}$$

$$\frac{1}{\pi}\left[\frac{\cos(\Phi/2) - \cos(\phi/2)}{1 - \cos(\phi/2)}\right]^{1/2}$$

for the two cases in equation (2), respectively.

Theoretical histograms based on equation (3), normalized to the area of 26 objects in the C histogram, and evaluated for $\Phi = 10^{o}$ are given in figure 6. Both histograms are more peaked than the observed data. Furthermore, the random-orientation model predicts less than 2 objects with $\phi > 20^{o}$ and the random alignment model predicts less than 4 objects, while the observations have found 10 objects (although 5 of the latter 10 are designated MULTIPLE). These two discrepancies between the model and the data may result from the following factors:

(1) measurement errors in width estimates and in the bin selection which would enter as a convolution of equation (2) with a function at least as broad as the peak;

(2) a range of values of $|\delta| = |\theta_o - \theta_m|$ from 0 to $(\Phi_o - \Phi_c)/2$ which would also tend to remove the sharp peak in figure 6 and which was purposely neglected;

(3) removal of assumption of a constant Φ, the physical cone width, which would again spread the peak. Models of Sturrock (1971) and Ruderman and Sutherland (1975) predict a dependence of Φ on spin frequency;

(4) a tendency for small values of θ_m which would increase the population at large values of ϕ;

(5) a multiplicity of closely spaced beams which would also increase the large-ϕ population; as noted, MULTIPLE profiles are included in the C histogram.

The theoretical S histograms should have a form similar to those in figure 6 with a smaller value for Φ and a broad convolving factor due to effect (2) above since $|\delta|$ varies from $(\Phi_o-\Phi_c)/2$ to $(\Phi_o+\Phi_c)/2$. The scaling of expected S widths, ϕ_S, to smaller ϕ-values than the DR widths, ϕ_{DR}, will be by a factor of

$$(4) \qquad \frac{\langle \phi_S \rangle}{\langle \phi_{DR} \rangle} = \left[\frac{4\,\Phi_c^{\,2} + 8\,\Phi_o\,\Phi_c}{3\Phi_o^{\,2} + 3\Phi_c^{\,2} + 10\,\Phi_o\,\Phi_c} \right]^{1/2}$$

as may be derived from the geometry of figure 1 and a uniform probability density for δ over the cone. For $\Phi_o = 7^o$ and $\Phi_c = 3^o$, values which are consistent with the bulk of the DR profiles, this ratio is 0.68. The S histogram in figure 5 has the form expected based on equation (2) and the discussion of a convolving factor (2) above, including the absence of objects large values of ϕ. However, the scale factor between the S and C histograms appears to be less than 0.5 -- the ratio of the medians is 0.4. The convolution effects (1-3) described above would not bias the median ratio, but the effects (4-5) would.

The models of Sturrock (1971) and Ruderman and Sutherland (1975) predict an elliptical hollow-cone beam with the major axis extending

along the sweep direction. However, the ratio $\langle\phi_S\rangle/\langle\phi_{DR}\rangle$ is not affected by the ellipse axial ratio. Finally, we mention that there may be a slight observational selection against very wide ($\gtrsim 90^\circ$) SINGLE profile since all pulsar searches seek radiation with many harmonics of a fundamental pulse period.

Based on the current hypothesis the DU profiles should also display a distribution similar to those in figure 6 with a scaling to smaller widths by the ratio

$$\frac{\langle\phi_{DU}\rangle}{\langle\phi_{DR}\rangle} = \left[\frac{16\,\Phi_o\,\Phi_c}{3\,\Phi_o^{\,2} + 3\,\Phi_c^{\,2} + 10\,\Phi_o\,\Phi_c}\right]^{1/2}$$

This ratio is 0.88 for $\Phi_o = 7^\circ$ and $\Phi_c = 3^\circ$. In fact the data in figure 5 show a ratio which exceeds unity, even when the questioned objects are excluded. Furthermore, the number of DU objects seems excessive based on the hypothesis that DU objects are those for which the observer axis just grazes the inside of the cone at the point of closest approach to the cone axis. By allowing physical cone dimensions Φ_o and Φ_c to vary amongst the sample of pulsars inspected, a large population of DU profiles can be created; the bias toward large ϕ would then be due to the difficulty of separating S and DU profiles with small ϕ.

IV. DISCUSSION

The analysis of the forms of pulsar radiation suggested in the introductory section and presented in §II compares favorably with the expectations of an hollow-cone beam model as shown in §III with a modest range of physical beam parameters (width, opening and axial ratio), with a random orientation of the observer and spin axes on the celestial sphere, with a random alignment of the cone and spin axes and with a small probability of multiple-beam objects. A number of the problems with the model are summarized in table 2 along with comments on the problems.

Obviously synoptic observations of pulsar waveforms over a wide frequency range would be of use in extending the quality and content of the data base presented in §II and the Appendix. The synthesis of pulsar waveforms presented here will be important in investigations of polarization phenomena where the "overlap" of unresolved components has observable consequences (Manchester et al. 1975). Finally items (2), (8) and (9) in table 2 constitute a challenge to current pulsar models.

The author wishes to thank his colleagues who participated in the observations discussed herein, the National Radio Astronomy Observatory and the National Research Council of the National Academy of Sciences

for support over the past four years and Professor M. Ruderman for illuminating discussions.

TABLE 1

PULSE PROFILE DATA SETS

Reference-Published Profiles	Radio Frequency(-ies)
Robinson et al. (1968)	5000 MHz
Gardner and Whiteoak (1969)	2650
Zeissig and Richards (1969)	111,611
Morris, Schwarz and Cooke (1970)	2695
Kommesaroff, Morris and Cooke (1970)	1720
Rankin et al. (1970)	430
Lyne, Smith and Graham (1971)	151,240,408,610
Manchester (1971a,1971b)	410,1665
Taylor and Hugennin (1971)	147
Backer (1972)	1400,4900
Wielebinski et al. (1972)	10690
Backer (1973)	318,430,611
Backer, Boriakoff and Manchester (1973)	430
Boriakoff and Payne (1973)	430,606
Crovisier (1973)	4850
Davies, Lyne, Skeiradis (1972,1973)	408
Downs, Reichley and Morris (1973)	2400,8400,15100
Backer, Rankin and Campbell (1975)	430

Table 1 (Continued)

Reference-Published Profiles		Radio Frequency(-ies)
Rankin and Campbell (1975)		430
Reference-Unpublished Profiles		
Authors	Investigation	
Craft (1970)	Ph.D. Thesis	40.1,111.5,196,318,430
Backer (1971)	Ph.D. Thesis	111.5,318,430,611
Backer and Fisher (1974)	Flux density	1392,2695,8085
Backer and Fisher (1975)	Flux density	
	[in 1971 (w. Manchester)]	116,147,196,224,1400
	[in 1973]	1392,2695,8085
	[in 1974]	775,968,1440
McCulloch (1974)		600-1400

TABLE 2

SUMMARY

PROBLEM	COMMENTS
1. Observed C width probability density is not sharply peaked.	(i) Measurement errors. (ii) Variable physical cone dimensions amongst the pulsar sample (see 7).
2. Large C population beyond 30°.	(i) Random alignment of cone axis and MULTIPLE beams. (ii) Alignment of cone axis favored.
3. Large DU population.	A range of physical cone parameters including $\Phi_o = \Phi_c$ which would remove the S/DU/DR distinction.
4. $\frac{\langle \phi_s \rangle}{\langle \phi_{DR} \rangle} < 0.5$	A bias in the DR sample toward large ϕ_{DR} (see 2).
5. Widths decrease slowly with ν.	Consistent with emission cone width scaling of Komesaroff (1970), Tademaru (1971) and Ruderman and Sutherland (1975).

TABLE 2 (Continued)

PROBLEM	COMMENTS
6. Widths decrease more slowly at high frequencies.	(see 5)
7. Spin frequencies of objects in the S/DU/DR categories are comparable, but there is a direct relation between width and spin frequency.	A natural feature of the emission-cone models of Sturrock (Roberts and Sturrock 1972, 1973) and of Ruderman and Sutherland (1975).
8. C objects often have a third component near the midpulse point with unique statistical properties.	A central pencil beam is unexplained in the present models.
9. Interpulses and emission bridges favored in rapidly rotating pulsars	(i) Width-spin relationship leads to increased detection probability (Roberts and Sturrock (1973)). (ii) Only one beam in the Ruderman and Sutherland model.

REFERENCES

Backer, D.C. 1970a, Nature, 227, 692.

_____. 1970b, ibid. 228, 1297.

_____. 1971, Ph.D. thesis, Cornell University, Ithaca.

_____. 1972, Ap.J. (Letters), 174, L157.

_____. 1973, Ap.J., 182, 245 (Paper I).

_____, Boriakoff, V., and Manchester, R.N. 1973, Nature Phys. Sci., 243, 77.

_____, and Fisher, J.R. 1974, Ap.J., 189, 137.

_____. 1975, in preparation.

_____, Rankin, J.M., and Campbell, D.B. 1975, Ap.J., 197, 481(Paper II).

Boriakoff, V., and Payne, R.R. 1973, Ap. Letters, 15, 175.

Cordes, J.M. 1975, Ap.J., 195, 193.

Craft, H.D., Jr. 1970, Ph.D. Thesis, Cornell University, Ithaca.

_____, and Comella, J.M. 1968, Nature, 220, 676.

Crovisier, J. 1973, Ap. Letters, 13, 221.

Davies, J.G., Lyne, A.G., and Skeiradis, J.H. 1972, Nature Phys. Sci., 240, 229.

_____. 1973, ibid., 244, 84.

Downs, G.S., Reichley, P.E., and Morris, D. 1973, Ap.J. (Letters), 181, L143.

Drake, F.D. 1968, Science, 160, 416.

Eastlund, B.J. 1968, Nature, 220, 1293.

Gardner, F.F., and Whiteoak, J.B. 1969, Nature, 224, 891.

Gold, T. 1968, Nature, 218, 731.

Gunn, J.E., and Ostriker, J.P. 1970, Ap.J., 160, 979.

Henry, G.R., and Paik, H-J. 1969, Nature, 224, 1189.

Hewish, A., Bell, S.J., Pilkington, J.D.H., Scott, P.F., and Collins, R.A. 1968, Nature, 217, 709.

Komesaroff, M.M. 1970, Nature, 225, 612.

_____, Morris, D., and Cooke, D.J. 1970, Ap. Letters, 5, 37.

Lyne, A.G. 1971, M.N.R.A.S., 153, 27p.

_____, Smith, F.G., and Graham, D.A. 1971, ibid., p. 337.

Manchester, R.N. 1971a, Ap.J. (Letters), 167, L101.

_____. 1971b, Ap.J. Supplement Series, 23, 283.

_____. 1971c, Ap.J. (Letters), 163, L61.

_____, Taylor, J.H., and Huguenin, G.R. 1975, Ap.J., 196, 83.

McCulloch, P. 1974 paper presented at Australian-United States Symposium on Pulsar Radiation Mechanisms, January 21-25, Stanford University, Palo Alto.

Morris, D., Schwarz, U.J., and Cooke, D.J. 1970, Ap. Letters, 5, 181.

Radhakrishnan, V., and Cooke, D.J. 1969, Ap. Letters, 3, 225.

Rankin, J.M., Comella, J.M., Craft, H.D., Jr, Richards, D.W., Campbell, D.B., and Counselman, C.C., III 1970, Ap.J., 162, 707.

_____, Heiles, C.E., and Comella, J.M. 1971, Ap.J.(Letters), 163, L95.

_____, Campbell, D.B., and Backer, D.C. 1974, Ap.J., 188, 609.

_____. 1975, in preparation.

Roberts, D.H., and Sturrock, P.A. 1972, Ap.J., 172, 435.

_____. 1973, ibid., 181, 161.

Robinson, B.J., Cooper, B.F., Gardner, F.F., Wielebinski, R., and Landecker, T.L. 1968, Nature, 218, 1143.

Ruderman, M., and Sutherland, P. 1975, Ap.J., 196,51.

Smith, F.G. 1972, Rep. Prog. Phys., 35, 399.

Sturrock, P.A. 1971, Ap.J., 164, 529.

Tademaru, E. 1971, Ap. and Sp. Sci., 12, 193.

Taylor, J.H., and Huguenin, G.R. 1971, Ap.J., 167, 273.

Wielebinski, R., Sieber, W., Graham, D.A., Hesse, H., and Schonhardt, R.E. 1972, Nature Phys. Sci., 240, 131.

Zeissig, G.A., and Richards, D.W. 1969, Nature, 220, 150.

APPENDIX

The forms of pulse profiles are discussed for 56 pulsars. Each is identified as SINGLE(S), DOUBLE/ UNRESOLVED(DU), DOUBLE/ RESOLVED(DR), TRIPLE(T) and MULTIPLE(M). The T objects are a subcategory of the DR objects as discussed in the text. A summary of this data is given in table A1.

PSR0031-07. DU based on an asymmetric extension of the profile on the trailing edge. The trailing half of the pulse has a steeper spectral index leading to the $\phi(\nu)$ curve in fig. 2b, is less polarized at 1400 MHz (unpublished observations), and has different P_3 fluctuations (Paper II).

PSR0138+59. DU based on profile observations from 775 to 1440 MHz.

PSR0301+19. DR based on profile observations (fig. 3). $\phi(\nu)$ varies as $\nu^{-0.15}$ in fig. 2c. Intensity fluctuations at 430 MHz (Paper II) and polarization at 430 MHz (Rankin and Campbell 1975) display the characteristic DR properties.

PSR0329+54. M based on extensive profile observations which have identified four components, three of which are comparatively weak (Lyne 1971, e.g.). $\phi(\nu)$ varies as $\nu^{-0.20}$ below $\sim$600 MHz and as $\nu^{-0.02}$ above 600 MHz. The average linear polarization profile is complex (Lyne et al. 1971).

PSR0355+54. DU based on a large variation of the spectral index in the two halves of the pulse which leads to the odd $\phi(\nu)$ curve in fig. 2b.

PSR0450-18. DU? based on profile and polarization at 408 MHz (Lyne et al. 1971) which suggest a non-SINGLE profile.

PSR0525+21. DR based on profile observations. $\phi(\nu)$ varies as $\nu^{-0.05}$ in fig. 2c; the peak separation has a slightly stronger dependence on radio frequency. Intensity fluctuations at 318 MHz (Paper I) and polarization waveforms near 400 MHz (Manchester 1971a, Rankin and Campbell 1975) display the characteristic DR properties. There may be a weak third component preceeding the pulse center (Paper I).

PSR0531+21. M based on profile observations from 318 to 611 MHz which indicate different spectral indices for the "precursor" component and the "mainpulse" and "interpulse" components (terminology of Rankin et al. 1969, see also Manchester 1971c and Rankin et al. 1971). The polarization states (Manchester 1971b) and the intensity fluctuations (Paper I) are also very different. The precursor/mainpulse separation is constant between 300 and 600 MHz. Pulsed radiation exists in the baseline between the mainpulse and interpulse.

PSR0540+23. S or DU depending on the significance given to the extension of the profile on the trailing edge at all frequencies studied (fig. 3). The central peak has a constant width over the range 430 to

1440 MHz (fig. 2a). Intensity fluctuations in the trailing edge are too weak to be studied (Paper II).

PSR0611+22. S based on profile observations.

PSR0628-28. S based on profile observations over a wide range of frequency (fig. 3).

PSR0736-40. DR based on profile observations near 1400 MHz (fig. 3). Further data may reveal a more complex waveform.

PSR0809+74. S or DU based on profile observations; at 151 MHz there is an asymmetric extension on the trailing edge of the pulse (Lyne et al. 1971) while near 1000 MHz their is an asymmetric extension on the leading edge which is intense enough to affect width measurements (fig. 2a). This description suggests two, or three, unresolved components with different spectral indices. The leading edge region is highly polarized at 1400 MHz (unpublished). The P_3 fluctuations are constant across the pulse.

PSR0818-13. S based on profile observations at 408 MHz.

PSR0823+26. S based on profile observations. $\phi(\nu)$ varies as $\nu^{-0.32}$ below 800 MHz and is constant above 800 MHz (table A1). There is a weak extension of radiation out to the component 32° following the pulse and an interpulse (Backer et al. 1973).

PSR0833-45. DU based on pulse width measurements from 834 to 8085 MHz (fig. 2b) which indicate that the two halves of the pulse have different spectral indices.

PSR0834+06. DR based on profile observations. The width is constant above 100 MHz (fig. 2c and table A1) unlike the characteristic DR case, although their may be an increasing width below 100 MHz. The intensity fluctuations (Paper I) and the polarization waveforms (Rankin et al. 1974) for this object are also not similar to the characteristic DR objects.

PSR0943+10. S based on profile observations and intensity fluctuations at 430 MHz (Paper II).

PSR0950+08. DR based on profile observations below 300 MHz where components I and II are resolved. $\phi_{DR}(\nu)$ varies as $\nu^{-0.55}$ below 300 MHz, while above 300 MHz the components are not resolved and $\phi_s(\nu)$ decreases with $\nu^{-0.05}$ (fig. 2c). At 430 MHz the two unresolved components are evident in polarization waveforms (Rankin and Campbell 1975) and in intensity fluctuations (Backer 1971). Pulsed radiation extends out on the leading edge all the way to the weak interpulse component (Paper II).

PSR1055-51. M based on profile observations. Both the "mainpulse" region and the "interpulse" region contain several components of comparable intensity (McCulloch 1974).

PSR1112+50. S based on profile observations.

PSR1133+16. DR based on profile observations, $\phi(\nu)$ varies as $\nu^{-0.25}$ below 600 MHz and as $\nu^{-0.10}$ above 600 MHz. Intensity fluctuations (Paper I) and polarization waveforms (Manchester 1971) display the characteristic DR properties.

PSR1237+25. T based on the similarity of components I, II, III and IV of this object (Backer 1970b) to the characteristic DR object. Component III in PSR1237+25 is identified with the central component of the TRIPLE profile (see schematics in fig. 1 and fig. 2d). The intensity fluctuations (Paper I) and polarization properties (Manchester 1971) are consistent with this description. ϕ (ν) decreases with $\nu^{-0.17}$ below 800 MHz and is constant above 800 MHz (table A1).

PSR1508+55. T based on profile observations. Below 500 MHz the central component (II) dominates the width measurements, while above 500 MHz, the intensity of the leading edge component(I) is comparable to that of II (see fig. 2d).

PSR1541+09. DR based on profile at 1440 MHz (fig. 4). Observations at 430 MHz indicate a MULTIPLE profile (Backer et al. 1973); however the most intense radiation arises in the regions identified by the peaks in fig. 4.

PSR1604-00. T based on profile observations (fig. 3) and on intensity fluctuations (Paper II). $\phi(\nu)$ varies as $\nu^{-0.05}$.

PSR1642-03. S based on profile observations of a constant-width, symmetric waveform.

PSR1706-16. S based on profile observations. The radio-frequency dependence of the width is uncertain.

PSR1749-28. S based on profile observations. The width is $4^{\circ}.6 \pm 0.2$ from 408 to 2695 MHz (not given in fig. 2a).

PSR1818-04. S based on profile observations. Below 500 MHz there is an asymmetric extension of the profile on the trailing edge which upon further investigation may place this object in the DU category.

PSR1826-17. DR based on profile observations between 775 and 1440 MHz.

PSR1831-04. M based on profile observations. The profile in figure 4 is nearly twice as wide as that given by Davies et al. (1973) at 408 MHz, which appears double. The additional width at 1440 MHz arises on the trailing edge based on our 775 MHz observation. Their may be six components at 1440 MHz.

PSR1845-04. S or DU based on profile observations between 775 and 1440 MHz. There is a weak asymmetric extension of the profile on the leading edge.

PSR1857-26. M based on profile observations at 408 MHz (Lyne et al. 1971) and 1400 MHz (unpublished). There appears to be five components in the profile.

PSR1859+03. DR based on profile at 1440 MHz. The relative intensity of one of the components decreases with decreasing frequency.

PSR1907+10. S based on profile observations.

PSR1911-04. S based on profile observations. Width is constant (fig. 2a and table A1).

PSR1915+13. S based on profile observations. Further investigation at 1400 MHz could lead to additional component on the trailing edge.

PSR1919+21. DR based on profile observations at high frequencies. Below 400 MHz only the leading edge component is evident, although there are additional "notches" in the average waveform (Cordes 1975) which are not considered here. The intensity fluctuations (Backer 1970a, 1973) display the characteristic DR properties, but the polarization properties do not.

PSR1929+10. T based on extensive profile observations and the intensity fluctuations near 430 MHz (Paper I). At 430 MHz components II and III are resolved, while at 111 MHz and at 2695 MHz components I and II are resolved. Consequently consistent width measurements are difficult; it appears that the width decreases with $\nu^{-0.25}$ (fig. 2d).

PSR1933+16. DU based on profile observations (fig. 3). The width is constant (fig. 2d and table A1).

PSR1944+17. DU based on profile observations (fig. 3) and intensity fluctuations at 430 MHz (Paper II). The width appears to increase with radio frequency (fig. 2b) which may indicate spectral index variations across the pulse.

PSR1952+29. DR based on profile observations.

PSR2002+31. S based on profile observations.

PSR2016+28. DU based on difference of radio spectrum in the two halves of the pulse which leads to the width variation in fig. 2b and on difference of P_3 fluctuations in the two halves (Paper I).

PSR2020+28. DR based on profile observations. The width varies as $\nu^{-0.05}$ (fig. 2c) which is similar to the characteristic DR objects, but the intensity fluctuations and polarization properties at 430 MHz (Paper II, Rankin and Campbell 1975, resp.) indicate more complex behavior. Note that this is also true for PSR0834+06 and PSR1919+21.

PSR2021+51. DR based on profile observations. The two components are of comparable peak intensity above 1000 MHz. $\phi(\nu)$ varies as $\nu^{-1.00}$ below 700 MHz and as $\nu^{-0.08}$ above 700 MHz where the components are not resolved.

PSR2045-16. T based on extensive profile observations. The polarization waveforms (Manchester 1971b) and the intensity fluctuations of components I and III (Taylor et al. 1971) display the characteristic DR properties. $\phi(\nu)$ varies with $\nu^{-0.15}$ below 1500 MHz (fig. 2d).

PSR2111+46. DR based on profile observations. The separation of the peaks varies as $\nu^{-0.25}$; the width displays a similar variation below 500 MHz and is constant above 500 MHz due to the radiation appearing

on the trailing edge (Backer et al. 1973). Further investigation may reclassify this object as MULTIPLE.

PSR2148+63. DU? based on profile observations between 775 and 1440 MHz. More accurate measurements are needed.

PSR2154+40. DU based on profile observations (fig. 3).

PSR2217+47. S based on profile observations from 147 to 1400 MHz. $\phi(\nu)$ varies as $\nu^{-0.07}$ (fig. 2a).

PSR2223+65. DR based on profile observations (fig. 3).

PSR2255+58. S based on profile observations.

PSR2303+30. S based on profile observations. The profile at 318 MHz is slightly asymmetric (Paper I).

PSR2319+60. T based on profile observations from 775 to 1440 MHz.

TABLE A1

SUMMARY

PSR	Period (ms)	Form	Half-Power Beamwidth (Deg)	Radio Frequency (MHz)
0031-07	943	DU	16.0±1.0	1000
0138+59	1223	DU	16. ±3.	1000
0301+19	1388	DR	14. ±1.	1000
0329+54	715	M	25. ±1.	1000
0355+54	156	DU	22. ±2.	1000
0450-18	549	DU?	19. ±1.	1000
0525+21	3745	DR	17. ±1.	1000
0531+21	33	M	28. ±2.	500
0540+23	246	S/DU	12.5±2.	1000
0611+22	335	S	8.5±0.5	500
0628-28	1244	S	18. ±2.	1000
0736-40	375	DR	21. ±1.	1000
0809+74	1292	S/DU	13. ±1.	500
0818-13	1238	S	7. ±1.	500
0823+26	531	S	3.0±0.2	1000
0833-45	89	DU	16. ±2.	5000
0834+06	1274	DR	7.6±0.4	1000
0943+10	1098	S	11.3±0.5	500
0950+08	253	DR	14. ±1.	1000
1055-51	197	M	27. ±3.	1000
1112+50	1656	S	5.8±1.0	1000
1133+16	1188	DR	8.4±0.4	1000
1237+25	1382	T	12. ±1.	1000
1508+55	740	T	11. ±1.	1000
1541+09	748	DR	74. ±10.	1000
1604-00	422	T	11. ±2.	1000
1642-03	388	S	3.7±0.3	1000
1706-16	653	S	6. ±1.	500
1749-28	563	S	4.6±0.2	1000
1818-04	598	S/DU	6.4±0.5	1000
1826-17	307	DR	16. ±2.	1000
1831-04	290	M	120. ±10.	1000
1845-04	598	S/DU	8. ±1.	1000

Table A1. (Continued)

PSR	Period (ms)	Form	Half-Power Beamwidth (Deg)	Radio Frequency (MHz)
1857-26	612	M	35. ±5.	1000
1859+03	655	DR	15. ±5.	1000
1907+10	284	S	8. ±3.	1000
1911-04	826	S	3.8±0.3	1000
1915+13	195	S	12.5±1.0	500
1919+21	1337	DR	9.2±0.2	1000
1929+10	227	T	13.5±2.	1000
1933+16	359	DU	6.4±0.3	1000
1944+17	441	DU	28. ±3.	1000
1952+29	427	DR	26. ±3.	1000
2002+31	2111	S	3.4±0.4	400
2016+28	558	DU	9.0±0.3	1000
2020+28	343	DR	13. ±1.	1000
2021+51	529	DR	8.7±0.5	1000
2045-16	1962	T	13.5±1.	1000
2111+46	1015	DR	44. ±4.	1000
2148+63	380	DU ?	10. ±2.	1000
2154+40	1525	DU	16. ±1.	1000
2217+47	538	S	7.2±0.4	1000
2223+65	683	DR	41. ±3.	1000
2255+58	368	S	12.7±1.0	1000
2303+30	1576	S	4.6±0.3	1000
2319+60	2256	T	18. ±2.	1000

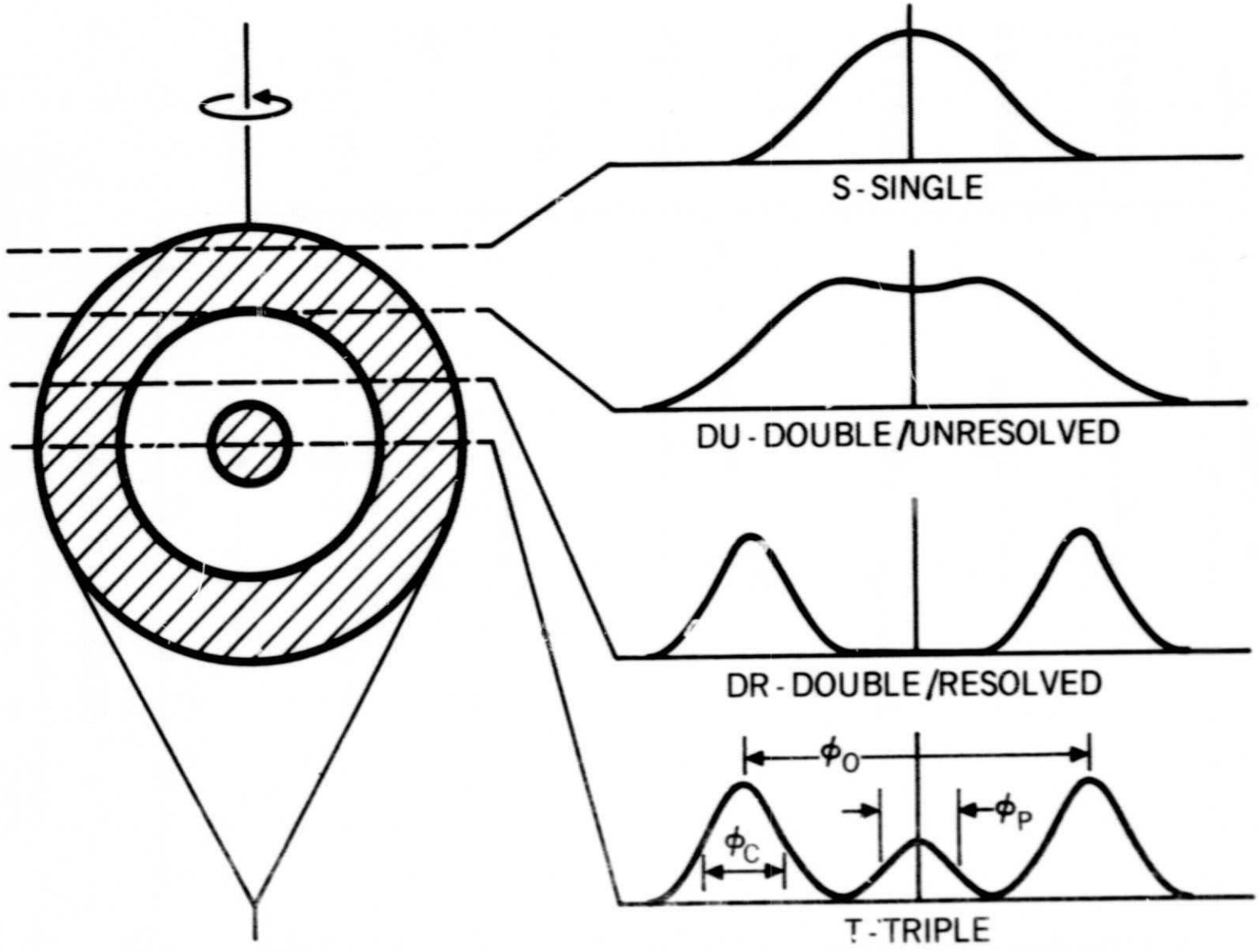

Fig. 1 Schematic of hollow-cone beam geometry (left) and the average waveforms that would be viewed by four observers with different inclinations from the rotation axis (right).

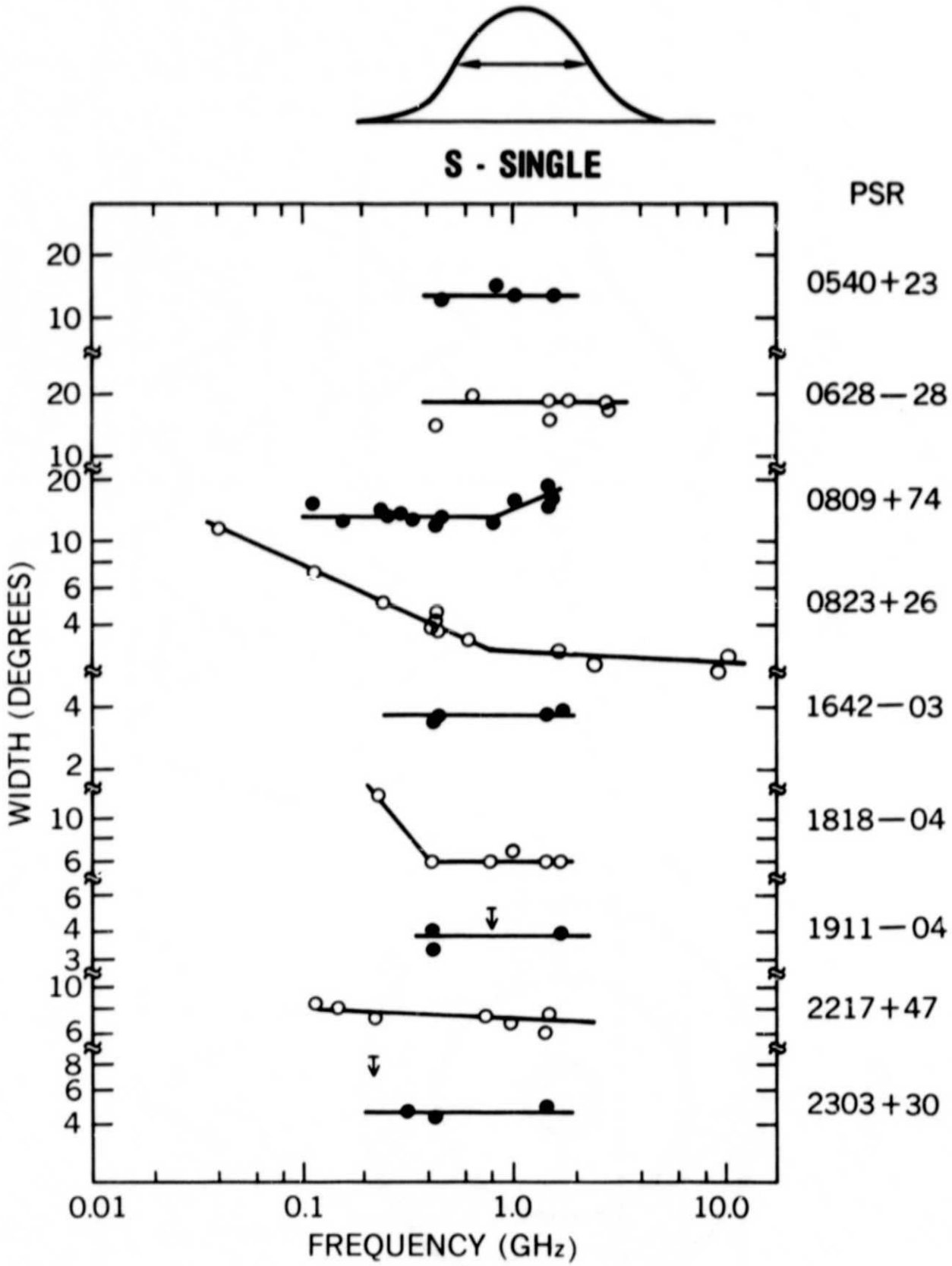

Fig. 2a Apparent half-power beamwidths of pulsars with SINGLE waveforms. Errors are generally less than 10 percent.

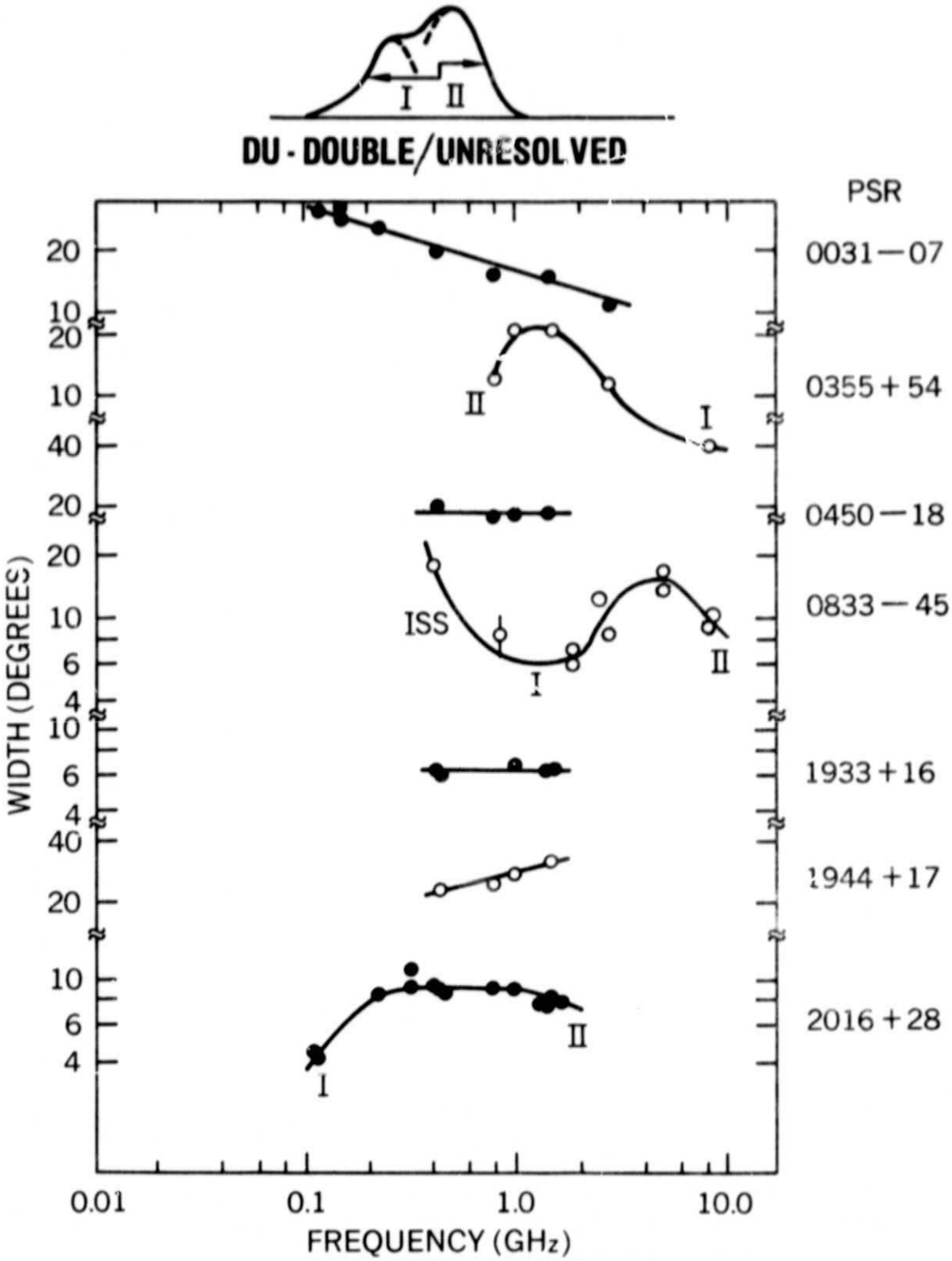

Fig. 2b Apparent half-power beamwidths of pulsars with DOUBLE/UNRESOLVED waveforms. Errors are generally less than 10 percent. Roman numerals indicate which of the two components identified in the schematic profile dominate the width measurements in certain domains of radio frequency.

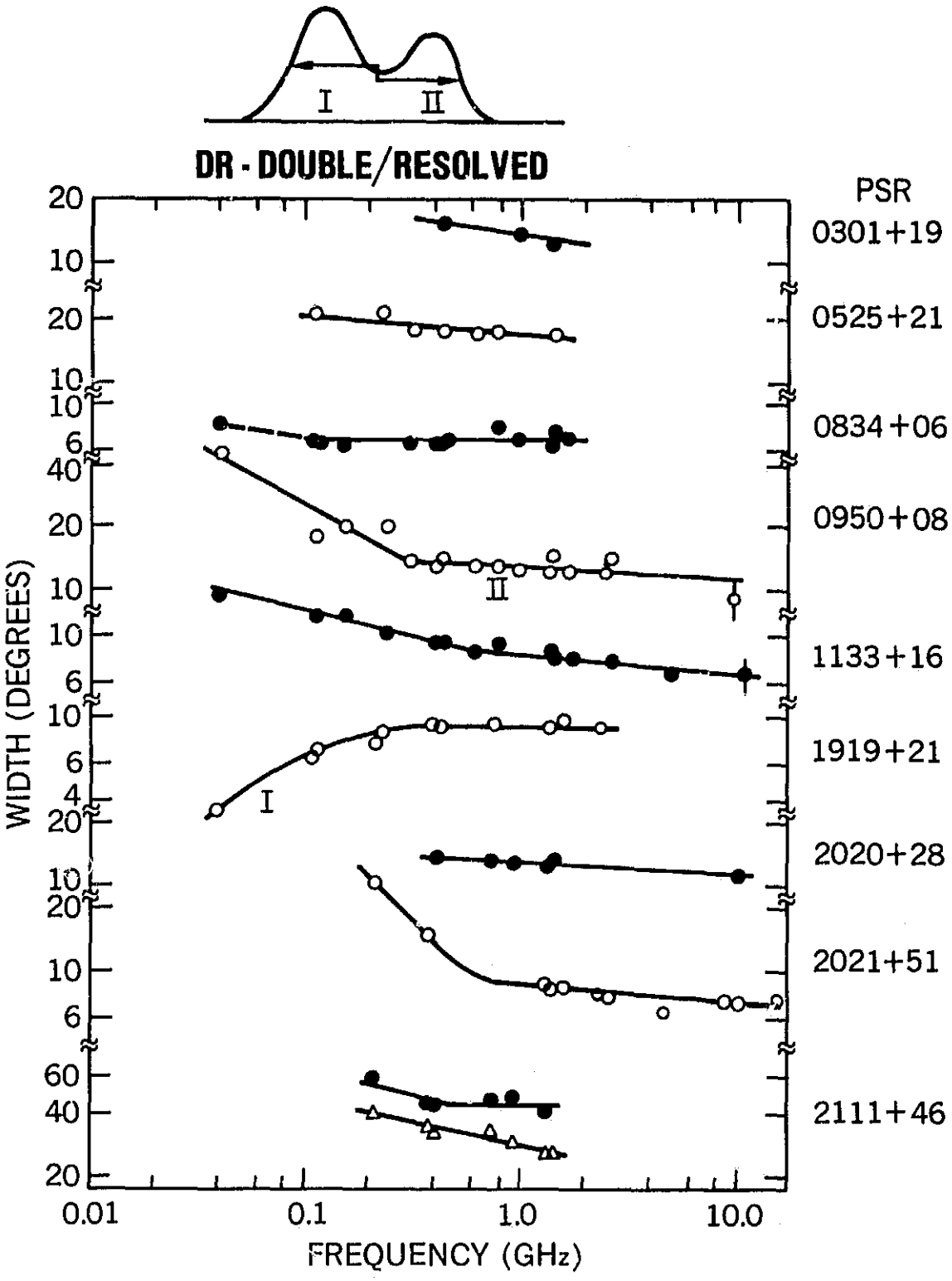

Fig. 2c Apparent half-power beamwidths of pulsars with DOUBLE/RESOLVED waveforms. See caption of fig. 2b for further details. The triangles below the widths of PSR2111+46 are measures of the peak separation (see Appendix for further comments).

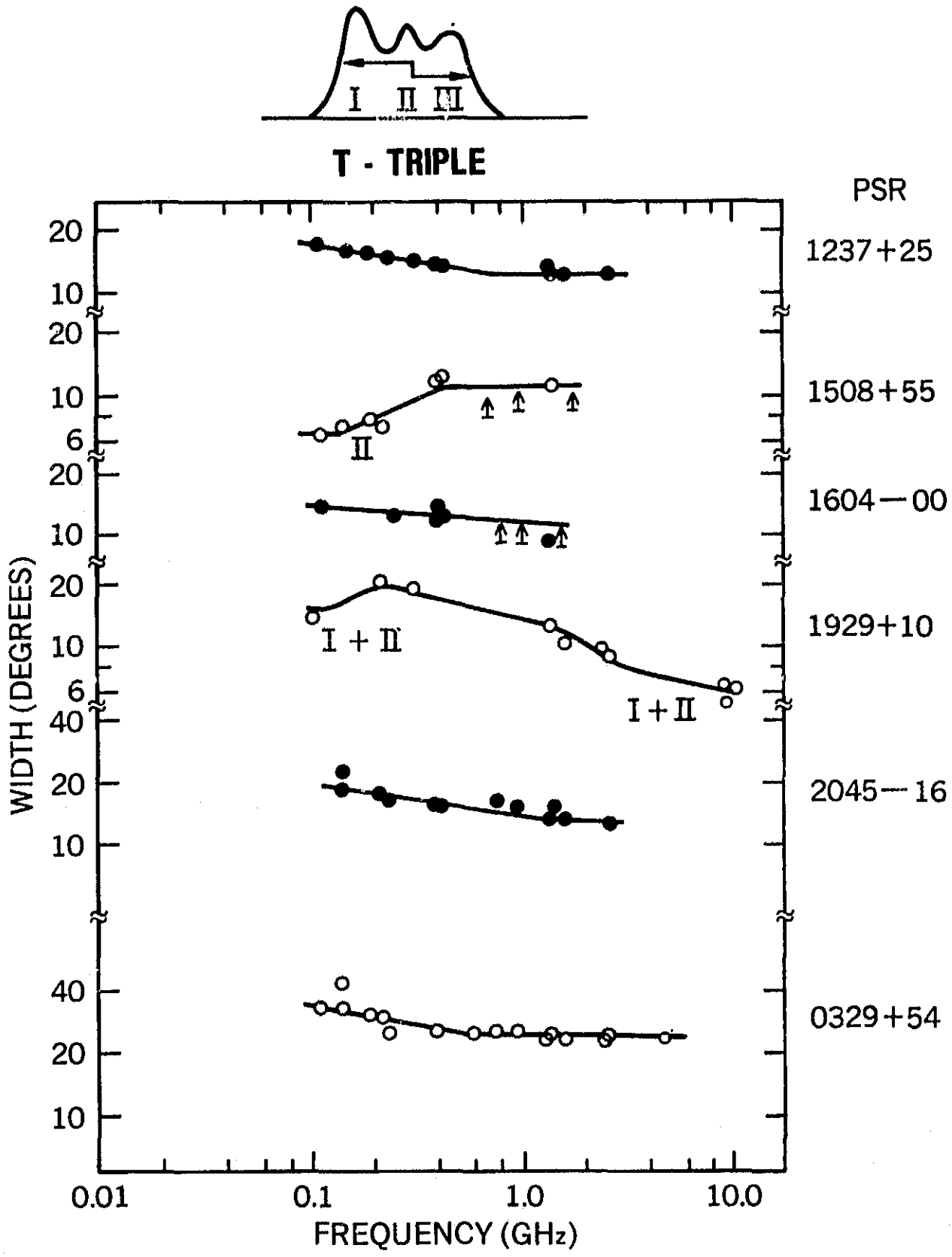

Fig. 2d Apparent half-power beamwidths of pulsars with TRIPLE waveforms. See caption of fig. 2b for further details. PSR0329+54, which has a MULTIPLE waveform, is included.

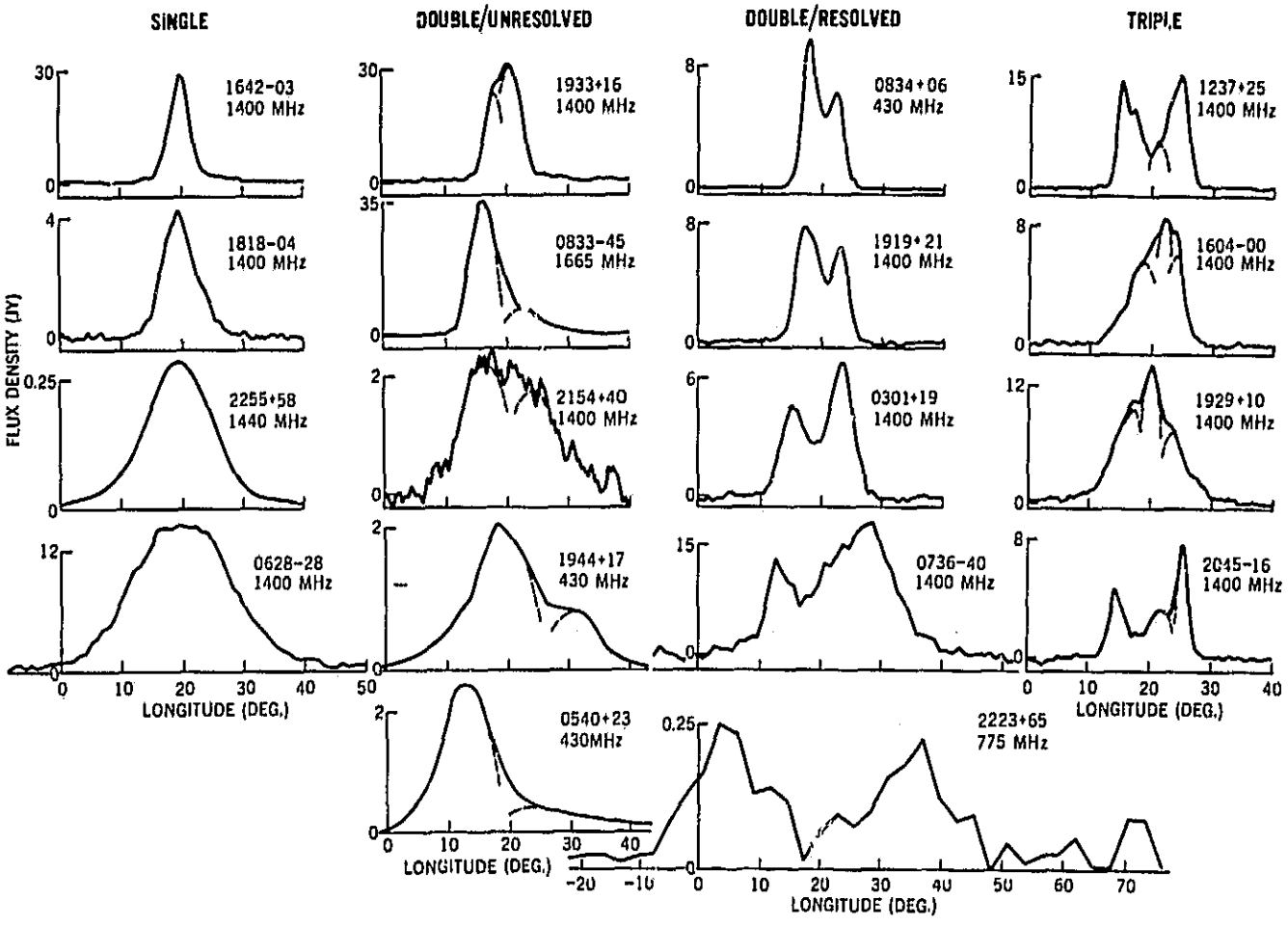

Fig. 3 Average, total-intensity waveforms of pulsars displayed in sequences of increasing apparent width for SINGLE, DOUBLE/UNRESOLVED and DOUBLE/RESOLVED categories, as well as a sequence of TRIPLE waveforms which have similar widths. The proposed components of the DOUBLE/UNRESOLVED and TRIPLE waveforms are delineated by dotted lines. Note that, as discussed in the text, component intensity ratios vary with radio frequency.

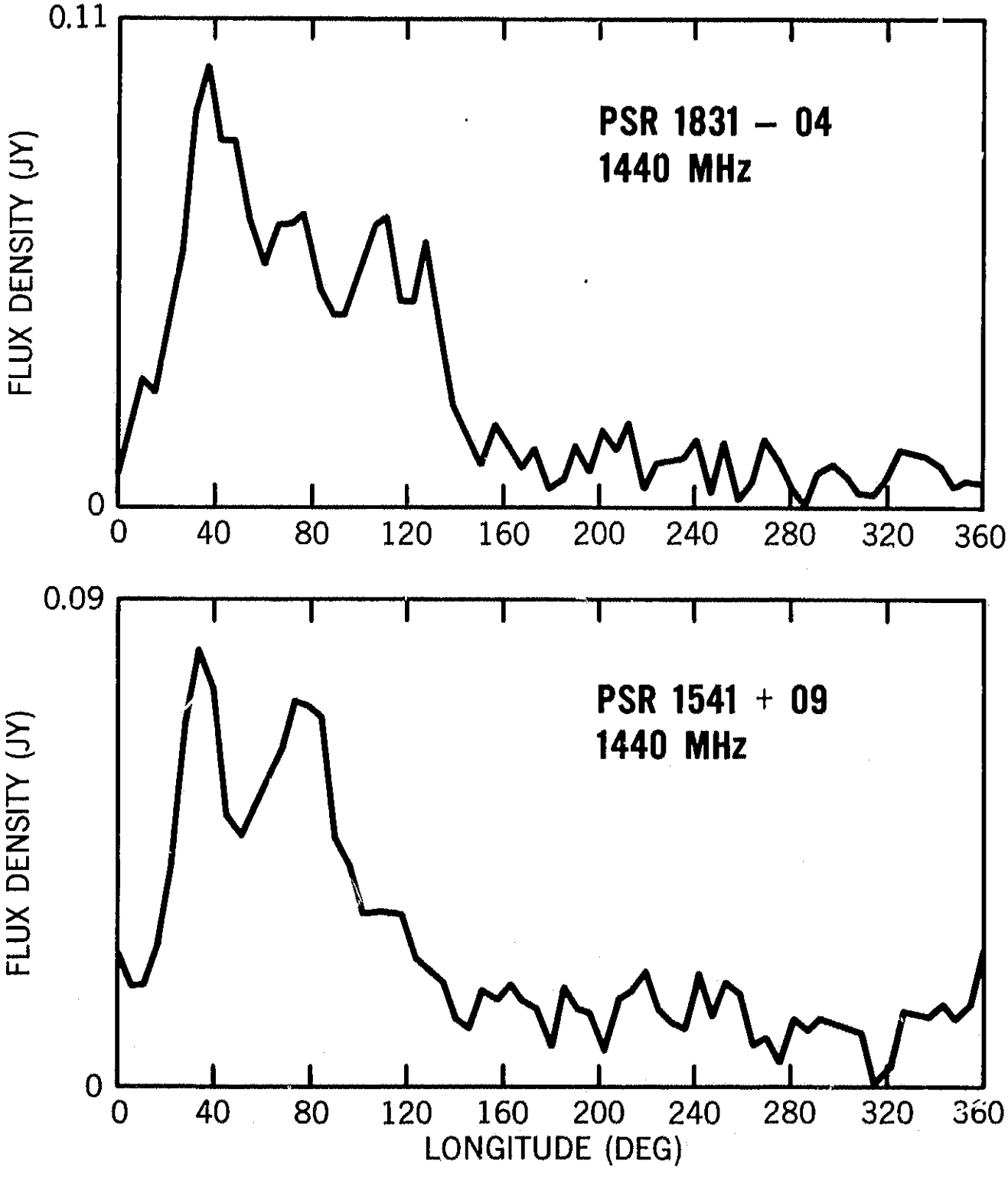

Fig. 4 Average total-intensity waveforms for two pulsars with exceptionally broad widths.

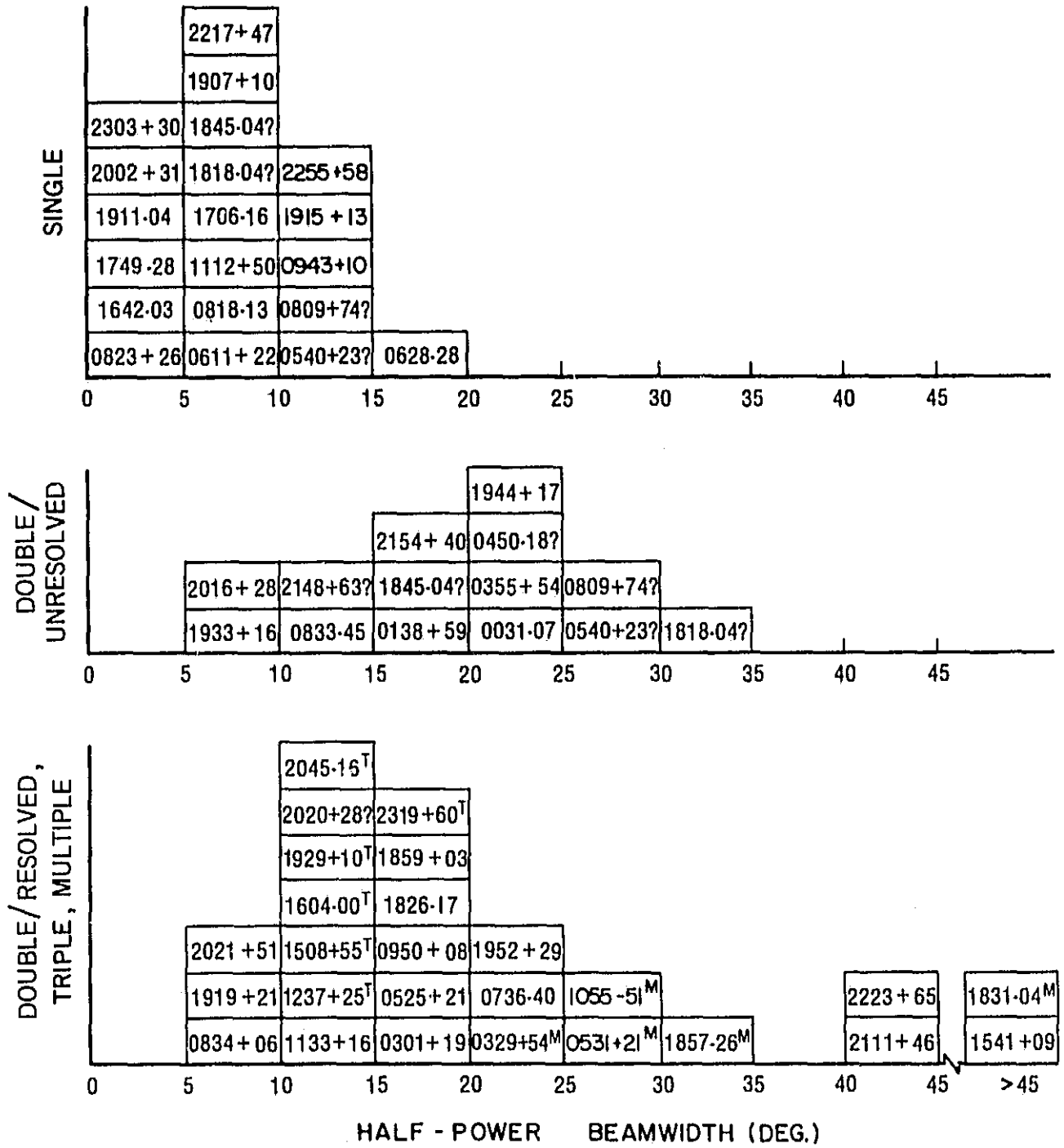

Fig. 5 Frequency of occurrence histograms for the three categories of pulsar waveforms discussed in the text. Questioned observations are indicated by ?; TRIPLE and MULTIPLE waveforms are indicated by the superscripts T and M, respectively.

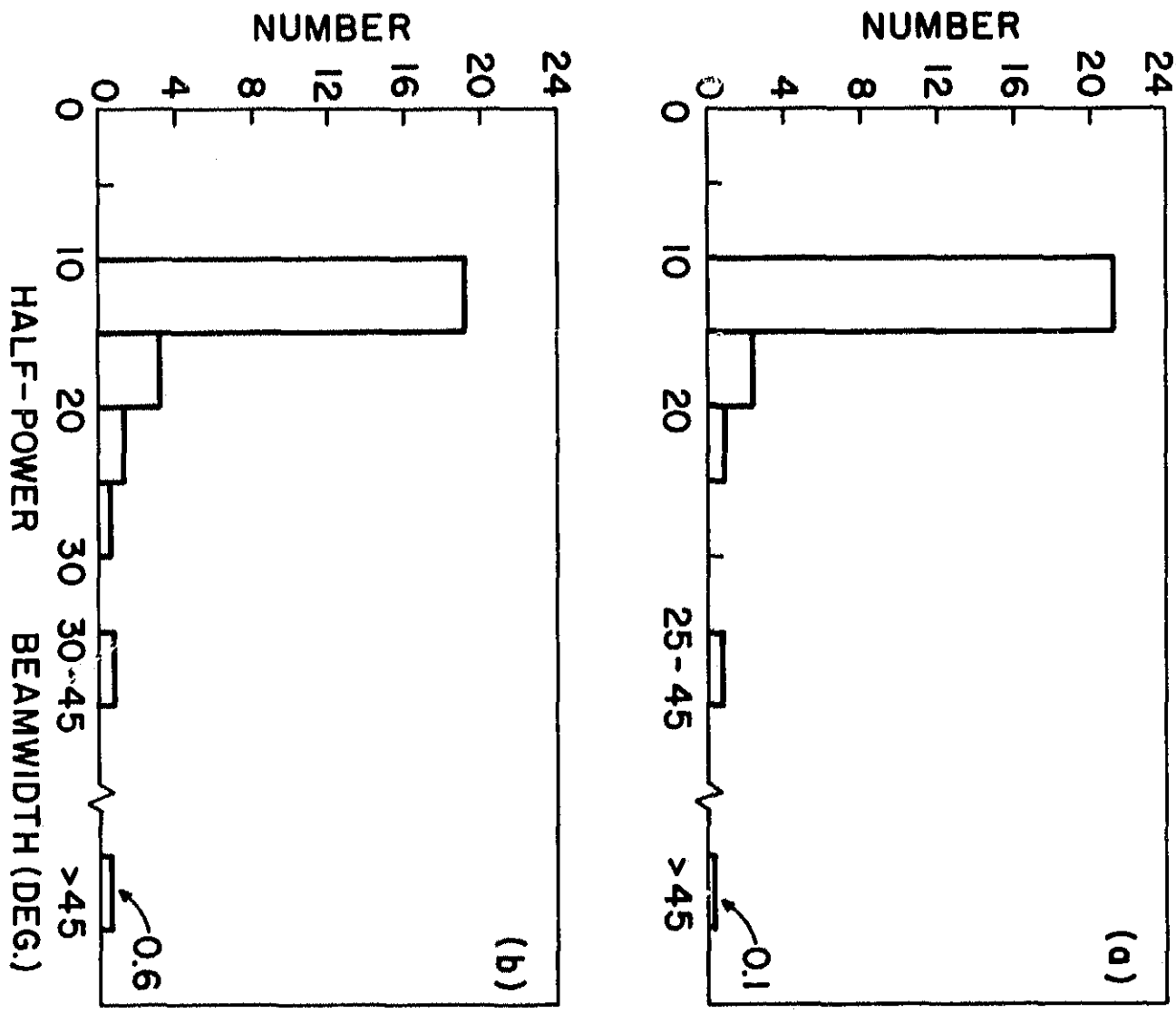

Fig. 6 Frequency of occurrence histograms for apparent widths of DOUBLE/RESOLVED waveforms in a circular, hollow-cone model with random observer-spin axis orientation and (a) random cone axis-spin axis orientation and (b) random cone axis-spin aixs alignment. The physical dimension of the cone is taken as 10 degrees. The areas are normalized to 26 objects.